Journal of Materials Chemistry B

Accepted Manuscript

ROYAL SOCIETY OF CHEMISTRY

www.rsc.org/materialsB

Journal Name Journal of Materials Chemistry B Dynamic Article Links ►

Cite this: DOI: 10.1039/c0xx00000x

www.rsc.org/xxxxxx

ARTICLE TYPE

Construction of cancer-targeted nanosystem as payload of iron complexes to reverse cancer multidrug resistance

Lilan Zeng, Jingjing Chen, Shengbin Ji, Leung Chan, Wenjie Zheng, Tianfeng Chen*

Received (in XXX, XXX) Xth XXXXXXXXX 20XX, Accepted Xth XXXXXXXXX 20XX

DOI: 10.1039/b000000x

Multidrug resistance has been identified as a major cause of failure of cancer treatment. Due to the relatively non-toxic ability, selenium nanoparticles (SeNPs) have been reported as an excellent cancer therapeutic nanodrug. In this study, we designed and prepared a novel nanosystem with borneol surface-functionalized and liver targeting to overcome the multidrug resistance. Borneol (Bor)-modified SeNPs can significantly improve the stability of SeNPs and improve the anticancer ability. $Fe(PiP)_3$ (PiP = 2-phenylimidazo [4,5-f][1,10] phenanthroline) is a novel anticancer agent with low solubility and stability. In this study, we have constructed a functionalized SeNPs (GAL/Bor@SeNPs) by surface decoration of galactosamine (GAL), a liver targeting ligand, which significantly enhanced the cellular uptake of $Fe(PiP)_3$-loaded nanosystem via dynamin-mediated lipid raft endocytosis and clathrin-mediated endocytosis in liver cancer cells overexpressing asialoglycoprotein receptor, thus achieving amplified anticancer efficacy. This multifunctional nanosystem exhibited excellent hemocompatibility and anticancer activity comparing with $Fe(PiP)_3$ or SeNPs alone. Remarkably, GAL/Bor@SeNPs antagonized the multidrug resistance in R-HepG2 cells by inhibiting the ABC family proteins expression, resulting in enhanced drug accumulation and retention. Internalized nanoparticles released free iron complexes into cytoplasm, which triggered ROS down-regulation and induced apoptosis through activating AKT and MAPKs pathways. Moreover, this nanosystem effectively prolonged the circulation time of encapsulated drugs.Taken together, this study suggests that GAL and Bor functionalization could be an effective strategy to design cancer-targeted nanomaterials to antagonize multidrug resistance in cancers.

1 Introduction

In recent years, nanotechnology-based chemotherapy has played an important role in cancer treatment.[1-3] However, mutidrug resistance limits the efficacy of chemotherapy.[4-6] It is well known that there are five categories main mechanisms of drug resistance: DNA repair activation, detoxification, decreased drug influx, increased drug efflux and blockage of apoptosis.[7] P-glycoprotein (P-gp or ABCB1) has been an important mechanism of multidrug resistance. P-gp, a ATP-dependent active efflux pump, can prevent chemotherapeutic drugs into the cell or discharged the drug from the cells.[8] Overcoming drug resistance is an essential factor to improve the efficacy of chemotherapy. To overcome the multidrug resistance, the current studies have used drug resistance inhibitors to block the specific efflux, or using agents to suppress the expression levels of the efflux proteins.[9] However, these studies were no significant treatment for the R-HepG2 cells with P-gp overexpressing. Therefore, it is necessary to develop a new nanoparticle with targeting liver cells for overcome the multidrug resistant in R-HepG2 cells.

The lipid solubility of chemotherapy drugs limits the efficacy of chemotherapy. Nanomaterials, with excellent solubility in water, can be used as drug carriers for cancer therapy to improve the efficacy of chemotherapy drugs.[10-12] Till now, a number of nanosystems, such as SeNPs, protein, oxides, polymers, and mesoporous silica, have been reported as drug carriers for cancer therapy.[13-15] Among these nanosystems, SeNPs, have been recently proposed as potential nanocarriers of chemotheraprutic agent owing to their excellent antioxidant properties, low-toxicity, high drug loading capability, excellent biocompatibility and degradability. In our previous study, we have showed that SeNPs could inhibit cancer cell growth by inducing cell apoptosis.[16-19] Therefore, SeNPs can be used as a vehicle for the treatment of cancer. Metal complexes, including copper (Cu), ruthenium (Ru), platinum (Pt), iron (Fe) and gold (Au), have been found demonstrated novel anticancer activities.[20-22] In recent years, a number of Fe complexes, owing to their interplay between chemical structure using diverse ligands, favorable cytotoxicity and the mechanism of DNA interaction against cancer cells, have been designed, synthesized and characterized as novel anticancer agents.[23-25] We found that, Fe complex $Fe(PiP)_3$ (PiP = 2-phenylimidazo [4,5-f] [1,10] phenanthroline),with an excellent anti-cancer activity for various cancer cells, could identified as novel broad spectrum of anticancer agents. However, the low aqueous solubility and toxicity of $Fe(PiP)_3$ was limited its further clinical application. Studies have showed that SeNPs exhibited application potential to delivery hydrophobic drugs into cancer

cells to overcome their low solubility and stability.[13, 26] The study use SeNPs as a drug delivery systems to overcome $Fe(PiP)_3$ insolubility and increase the loading rate of $Fe(PiP)_3$.

Borneol (Bor) is a bicyclic monoterpenoid alcohol with antibacterial and anti-inflammatory effects.[27] Interestingly, borneol was found be able to penetrate the blood-brain barriers (BBB), to improve some drug's oral bioavailability, and to increase the drug distribution in brains.[27, 28] Particularly, borneol has been reported use as a biological active substance in the cell signaling transduction, and could improve the cellular uptake of organic Se compounds in cancer cells and enhance its anticancer efficacy through inducing apoptosis.[29] Furthermore, borneol can participate in reversing multidrug resistance by inhibition the expression of p-gp.[30, 31] Moreover, in order to overcome the multidrug resistance, most of current studies used targeting drugs for cancer chemotherapy, such as folate acid, TAT, transferring, RGD, HER-2 and lactobionic acid.[32-34] Many studies have been carried out to discover strategy to enhance drug delivery to livers. These carriers target to human hepatoma cell lines based on hepatic receptor recognition.[35-37]Asialoglycoprotein receptors (ASGP R), which were well-known surface receptors exists only in hepatocytes cell lines, were able to recognize and bind molecules having exposed N-acetylgalactosamine, galactose, or glucose residues.[34, 38] Therefore, many studies have utilized asialoglycoprotein receptor-mediated drugs into liver cells because the asialoglycoprotein receptor has a high combination capacity and can effectively improve cellular uptake of galactosylated ligands.[39, 40] In this study, we have designed a novel cancer-targeted drug carrier SeNPs by using Bor to enhance membrane permeability and GAL as a liver cancer targeting ligand, as payload of $Fe(PiP)_3$ as a anticancer metal complex. Our results showed that, this multifunctional nanosystem could improve the capacity of $Fe(PiP)_3$ in cellular uptake and anticancer efficacy to overcome the multidrug resistance in cancer cells. And then the underlying molecular mechanisms accounting for the anticancer effects were also examined in detail. In summary, this study provides a strategy for rational design and construction of functional nanosystem to reverse multidrug resistant cancers.

2 Materials and methods

Materials

Galactosamine hydrochloride (GAL) was purchased from Aladdin, and other chemicals was obtained from Sigma-Aldrich.

Preparation and characterization of the nanosystem

The preparation of GAL/Bor@SeNPs were performed following our previously study.[26] For GAL conjugation, 10 μL of thioglycolic acid (TGA) solution was stirred with GAL for overnight by using EDC and NHS as amidation catalyst. A 0.8 mL aliquot of ascorbic acid (VC) solution was mixed with $Fe(PiP)_3$ (300 μL, 10 mg/mL) , then Na_2SeO_3 was added to the reaction solution dropwise, and reacted for 30 min, then added Borneol (Bor) solution (100 μL of 12.34 mg) and GAL-TGA solution (200 μL, 5 mg/mL). The mixed solution was volumed to 10 mL with Milli-Q water. After reaction, the dialysis experiments were taken in Milli-Q water to remove the excess $Fe(PiP)_3$ and Na_2SeO_3. The concentration of Se and Fe was evaluated by ICP-MS analysis and UV-vis spectroscopy, respectively. To estimate the drug encapsulation efficiency of $Fe(PiP)_3$ in this nanosystem, the nanoparticles was examined with UV-vis spectroscopy measurement using a standard curve method (λ=534 nm).

The GAL/Bor@SeNPs were characterized by different spectroscopic and microscopic measurements, such as UV-vis spectroscopy (Carry 5000), FT-IR (Equinox 55 IR), TEM (Hitachi H-7650), Zetasizer particle size analysis (Malvern Instruments Limited), fluorescence spectroscopy analysis.

Hemolysis assay

The hemolysis of red blood cells exposed to SeNPs, Bor@SeNPs, $Fe(PiP)_3$ and GAL/Bor@SeNPs were investigated by spectrophotometry.[41] To evaluate the erythrocyte agglutination, the red blood cells were incubated with each sample (20 μL) for 2 h, then placed onto glass slide, covered and observed under microscope (Life technologies, EVOS FL auto).[42]

Cell culture and MTT assay

HepG2 hepatocellular carcinoma cells, HepG2 drug resistant hepatocellular carcinoma cells (R-HepG2) cells and LO2 normal hepatocyte, were obtained from American Type Culture Collection (ATCC, Manassas, Virginia), and cultured in DMEM medium and R-HepG2 cells were incubated in1640 medium. The medium was supplemented with streptomycin (50 units/mL), penicillin (100 units/mL) and FBS (10%) at 37 ℃ in a humidified incubator with 5% CO_2. To examine the relative cytotoxicity of GAL/Bor@SeNPs in vitro, we determined it by a MTT assay toward HepG2, R-HepG2 and LO2 cells. The cell growth inhibitory effects of the nanosystems on different cells were examined by MTT assay as previously decribed.[2]

In vitro cellular uptake of GAL/Bor@SeNPs

To quantify the cellular uptake of 6-coumarin-loaded GAL/Bor@SeNPs, the fluorescence microplate reader was taken with ex/em set at 430 and 485 nm respectively.[17]

Asialoglycoprotein competing assay

Generally, GAL/Bor@SeNPs will recognize the GAL receptor asialoglycoprotein (ASGP R), and therefore excess amount of GAL could compete with the nanoparticles to bind ASGP R expressed in R-HepG2 cells. Thus, the ASGPR competing assay was examined by fluorescence microplate reader to determine the cellular uptake of the nanaparticles.[19]

Intracellular trafficking of GAL/Bor@SeNPs

The intracellular trafficking of the nanosystem in R-HepG2 and HepG2 cells was treated with the nucleus marker DAPI and the lysosomal marker Lyso Tracker Red monitored by fluorescence microscopy (IX51, Olympus) as previously described.[43]

Cellular uptake pathways of GAL/Bor@SeNPs

As our previous study, inhibitors of endocytosis, including 2-deoxy-Dglucose (DOG) (50 mM), dynasore (80 mM), sucrose (0.45 mM), sodium azide (NaN_3) (10 mM), and nystatin (10 μg/mL), were used to estimate the cellular uptake pathways of GAL/Bor@SeNPs in R-HepG2 cells.[17] The fluorescence intensity of coumarin-6-loaded GAL/Bor@SeNPs with ex/em wavelengths

set at 430 and 485 nm was measuring by fluorescence microplate reader (Spectra Max M5, Bio-Tek). The concentration of couramin-6 probe in the nanoparticles was found at 2.74 μg/mL.

***In vitro* drug release of GAL/Bor@SeNPs**

The drug release of GAL/Bor@SeNPs was measured as our previously described.[3] The concentration of $Fe(PiP)_3$ was examined by UV-vis spectrum with wavelength set as 534 nm.

Flow cytometric analysis

PI-Flow cytometry analysis was used to determine the effects of GAL/Bor@SeNPs on the cell cycle distribution of cancer cells.[18]

Determination of reactive oxygen species (ROS) level

The effects of GAL/Bor@SeNPs on the intracellular ROS level in cancer cells were investigated by using fluorescence DHE assay as previously described.[19] In order to further examine the GAL/Bor@SeNPs could induce the variation of ROS, R-HepG2 cells were seeded in 2-cm dish and labelled with 10 μM DHE at 37 ℃ for 30 min. After that, the cells were observed by fluorescence microscopy at different times.

Western blot analysis

The R-HepG2 cells were treated with different concentration of GAL/Bor@SeNPs for 72 h, then incubated in cell lysis buffer (Beyotime) for 10 min to extract the total cellular proteins. The effects of GAL/Bor@SeNPs on the expression levels of proteins related with different cell signaling pathways were examined by Western blotting.[44, 45]

***In vivo* pharmacokinetic assay**

Pharmacokinetic assay was used to examine the effect of GAL/Bor@SeNPs in blood circulation as previously described.[46] Female Sprague Dawley (SD) mice (about 190-210 g) used in this study were obtained by the Medical Laboratory Animal Center of Guangdong provice. The mice were in-house cage with a standard conditions and standard diet. Six mice were randomly assigned to two groups. Mice were fasted overnight before the experiment. The dose of $Fe(PiP)_3$ and GAL/Bor@SeNPs was 5 mg/kg of mouse body weight (n = 3 per group) through intravenous injection. At different time points (0, 0.0083, 0.5, 1, 2, 4, 8, 12 and 24 h), the blood samples were collected from retro-orbital plexus, then centrifuged (3000 rpm, 10 min) to obtain plasma. The $Fe(PiP)_3$ was extracted by dissolving blood samples in HCl (0.75M)/isopropanol at -20℃ overnight. Then the samples were centrifuged at 12000 rpm for 20 min and the amount of Fe in the plasma was evaluated by UV-vis. The plasma clearance (Cl) and the area under the blood concentration curve (AUC), which were the main pharmacokinetic parameters, were calculated by using winonlin 3.3 software.

Biodistribution study

The mice were fed with $Fe(PiP)_3$ and GAL/Bor@SeNPs at dosage of 5 mg/kg of mouse body weight (n=3 per group) through intravenous administration, and then sacrificed at 72 h and the organs including heart, liver, spleen, lung and kidney were obtained. The drug concentration of Fe complex in each organ was determined by using UV-vis as described above.

Statistical Analysis

All experiments were carried out at least in triplicate and results were expressed as mean ± S.D. The difference between different groups was analyzed by one-way ANOVA multiple comparisons. Difference with $P < 0.05$ (*) or $P < 0.01$ (**) was considered statistically significant.

3 Results and discussion

Rational design, preparation and characterization of GAL/Bor@SeNPs

The study describes the design of GAL-conjugated SeNPs as cancer-targeted drug delivery system for $Fe(PiP)_3$ to overcoming the multidrug resistance. Bor, a traditional Chinese medicine, also be used as an enhancer of drug absorption.[47] Therefore, the Bor can increased the stability of SeNPs and increase the absorption of $Fe(PiP)_3$. GAL-targeted SeNPs, with ASGP R-mediated endocytosis, can antagonize the multidrug resistant by increasing the cellular uptake of drugs. Here, we have prepared GAL/Bor@SeNPs as illustrated in **Fig. 1A**. In our study, Bor was used as a surface modifying agent for SeNPs to increase its stability and acted as an enhancer of drug absorption. As shown in **Fig. 1B**, the average diameter of SeNPs maintained at about 520 nm without Bor surface modification, which should be due to the instability and rapid deposition of SeNPs. Interestingly, the use of Bor can significantly reduce the particle diameters of SeNPs. While the concentration of Bor at 0.31-2.48 mg/mL, the particle diameters of SeNPs were 183, 162, 125, 157, 298 nm, respectively. It is important that the stability of nanoparticles is one of fundamentally tissues for evaluating their medical applications. Moreover, in aqueous solution, the size of GAL/Bor@SeNPs kept constant with an average size of 150 nm in 40 days, which increased gradually afterward. TEM images show that the GAL/Bor@SeNPs was almost spherical and with a diameter of about 30-80 nm (**Fig. 1E**). The results were consistent with the particle size in aqueous solutions (**Fig. 1D**). As shown in **Fig. 1F**, the zeta potential of SeNPs was -9.3 mv. However, after conjugation of Bor and continuous loading of $Fe(PiP)_3$, the zeta potential was further decreased to -43.7 and 33.9 mv. It shows that surface modified Bor can increase the stability of nanoparticles. This excellent stability of GAL/Bor@SeNPs support their future medical application.

As demonstrated in the results of FT-IR, the appearance of peak at 2975.34 cm^{-1} corresponded to the stretching vibration of C-H from Bor and peak at 1457 cm^{-1} corresponded to the benzene ring from $Fe(PiP)_3$ in the spectrum of GAL/Bor@SeNPs supported the successful decoration of Bor and loading to the drug $Fe(PiP)_3$ (**Fig. 2A, Fig. S1**). The finding of peaks at 1626.75 and 1546 cm^{-1} of amide bands I and amide bands II from GAL indicated the successful conjugation of GAL to the nanoparticles. Consistently, as shown in the results of UV-Vis spectra (**Fig. 2B**), the changes in the spectra of SeNPs, Bor@SeNPs and GAL/Bor@SeNPs further confirmed the successful decoration of Bor and GAL on the nanoparticles. The appearance of characteristic peak of $Fe(PiP)_3$ in the spectrum of GAL/Bor@SeNPs demonstrated the successful drug loading of $Fe(PiP)_3$. Moreover, the drug encapsulation efficiency of $Fe(PiP)_3$ in the nanosystem was found at 37.3%, as determined by UV-vis analysis.

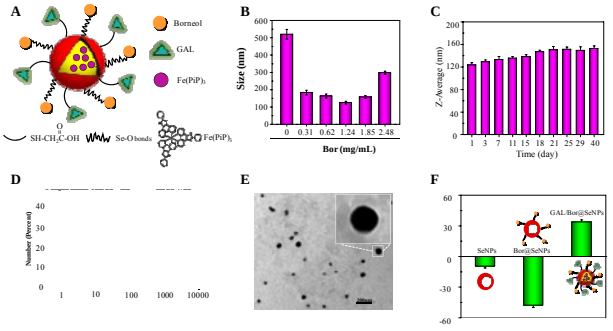

Fig. 1 Structural characterization of GAL/Bor@SeNPs. (A) Schematic illustration of GAL/Bor@SeNPs. (B) Bor@SeNPs particle diameters at various concentrations of Bor at 24 h. (C) Stability of GAL/Bor@SeNPs in aqueous solutions. (D) Size distribution of GAL/Bor@SeNPs in aqueous solutions. (E) TEM image of GAL/Bor@SeNPs, scale bar 200 nm. (F) Zeta Potential of SeNPs, Bor@SeNPs and GAL/Bor@SeNPs. Each value represents means ± SD (n=3).

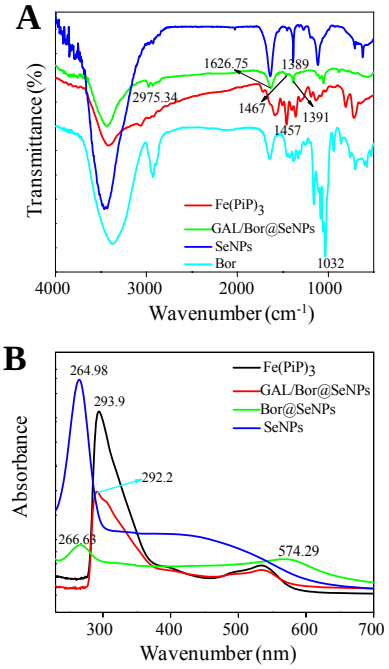

Fig. 2 (A) FT-IR spectra of $Fe(PiP)_3$, GAL/Bor@SeNPs, SeNPs and Bor. (B) UV-vis spectra of $Fe(PiP)_3$, GAL/Bor@SeNPs, Bor@SeNPs and SeNPs.

Hemocompatibility of GAL/Bor@SeNPs

As we all known, the biocompatibility of drug plays an important role in drug delivery applications. Excellent hemocompatibility of drug delivery is a crucial factor because nanodrugs are typically into the body through intravenous infusion in the clinical. In this experiment, to estimate the hemocompatibility, the hemolysis assay was taken. The RBCs was subjected to different sample of different concentration for 10 min and 2 h. As shown in **Fig. 3A** and **Fig. S2**, the Hemolysis Rate (HR) of SeNPs and Bor@SeNPs were none hemolytic (less than 5%) even at high concentration of 30 μM. As shown in **Fig. 3B** and **Fig. S2**, compare with GAL/Bor@SeNPs, the HR of $Fe(PiP)_3$ was out of range. When RBCs was exposed to the GAL/Bor@SeNPs and $Fe(PiP)_3$ for the

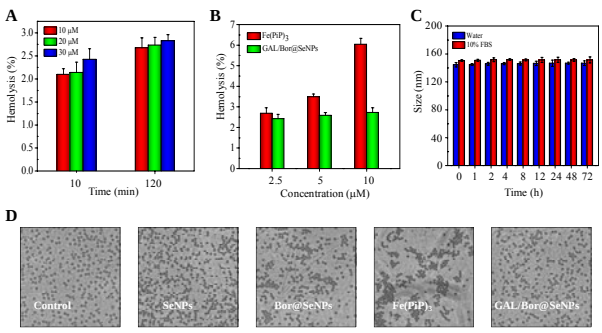

Fig. 3 Hemocompatibility of SeNPs, Bor@SeNPs, $Fe(PiP)_3$ and GAL/Bor@SeNPs. (A) Percentage of RBCs hemolysis incubated by SeNPs for 10 min and 120 min. (B) Percentage of RBCs hemolysis incubated by different concentrations of $Fe(PiP)_3$ and GAL/Bor@SeNPs for 120 min. (C) Changes in the particle size of GAL/Bor@SeNPs in water and FBS. (D) Agglutination of human erythrocytes by SeNPs, Bor@SeNPs, $Fe(PiP)_3$ and GAL/Bor@SeNPs. Each value represents means ± SD (n=3).

same concentration in 2 h, the HR of GAL/Bor@SeNPs was 2.72%, while $Fe(PiP)_3$ was 6.09% . In addition, after exposed to these drugs for 2 h, all the sample induced slight agglutination of the RBCs except the $Fe(PiP)_3$. As shown in **Fig. 3D**, there is a significant agglutination through by $Fe(PiP)_3$. Since the cell membrane is negatively charged, positively charged nanoparticles can be more effectively to enter into the cells.[48] However, the particles have a positive surface charge makes it difficult for in vivo applications, especially intravenously. It is possible that the nanoparticles with positive charge may be rapidly cleared out from the blood circulation for the intravenous injection. Therefore, the stability of nanoparticles in 10% fetal bovine serum (FBS) and aqueous solution was examined. As shown in **Fig. 3C**, the particle size of GAL/Bor@SeNPs in water with a slight increase after 72 h. Moreover, the particles in FBS (about 152 nm) were slightly larger than those in aqueous solution (about 147 nm), which may be due to the nonspecific interactions of GAL/Bor@SeNPs and serum proteins. Taken together, these results demonstrate that GAL/Bor@SeNPs display high hemocompatibility and high stability in both aqueous and serum condition, which could support their future medicinal application.

Selective cellular uptake of GAL/Bor@SeNPs

Nanoparticles with size less than 200 nm are more likely to enter the cell, and thus increase the selectivity of the drug in cancer cell.[43] In our study, we have prepared the nanoparticles with size from 30 to 80 nm. Therefore, GAL/Bor@SeNPs can use as a useful therapeutic drugs to cancer cells. In our work, the GAL/Bor@SeNPs surface-functionalized with GAL could specifically recognize the ASGP R receptor overexpressed in hepatocellular carcinoma cells membrane, which could facilitate the interaction of the nanoparticles with the cells and enhance their cellular uptake through active targeting process.[49] In order to investigate the contribution of ASGP R in the cellular uptake of GAL/Bor@SeNPs, the expression levels of ASGP R in the tested cancer cell lines were investigated. **Fig. 4B** showed that the expression levels of ASGP R in R-HepG2 and HepG2 cells were significantly higher than that in LO2 cells and the expression levels of ASGP R in R-HepG2 cells was higher than in HepG2 cells. These results show that the GAL surface decoration

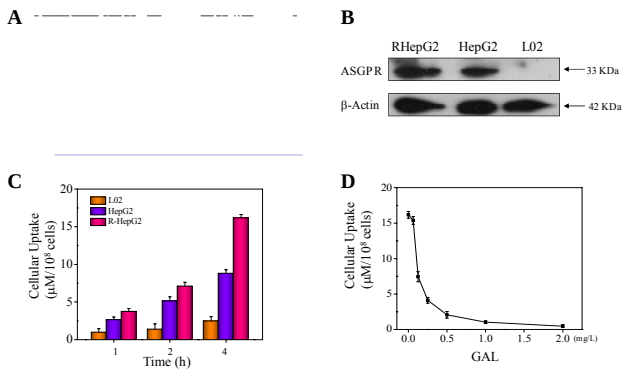

Fig. 4 Selective cellular uptake of GAL/Bor@SeNPs. (A) The schematic of selective cellular uptake by ASGP R. (B) ASGP R expression in HepG2 cells, R-HepG2cells and LO2 cells. The expression level of ASGP R was evaluated by western blot analysis. β-Actin was used as loading control. (C) Quantitative analysis of cellular uptake efficiency of 6-coumarin loaded GAL/Bor@SeNPs (30 μM) in LO2, HepG2 and R-HepG2 Cells. (D) Concentration-dependent effects of GAL on the cellular uptake of GAL/Bor@SeNPs. The cells were exposed to various concentrations of GAL for 2 h, and then incubated to 30 μM GAL/Bor@SeNPs for 4 h. Each value represents means ± SD (n=3).

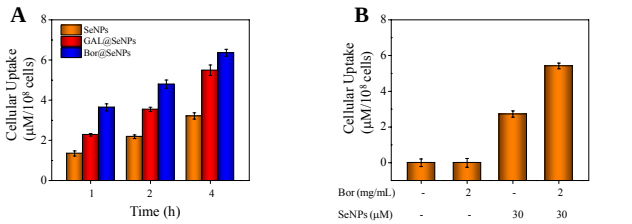

Fig. 5 Bor and GAL enhances the cellular uptake of SeNPs on R-HepG2 cells. (A) Quantitative analysis of cellular uptake efficiency of 30 μM 6-coumarin loaded SeNPs, Bor@SeNPs and GAL@SeNPs. (B) Quantitative analysis of cellular uptake of 6-coumarin loaded SeNPs (30 μM) into cells exposed to 2 mg/mL Bor and 30 μM SeNPs. The cells were pretreated with Bor for 12 h, and then exposed to SeNPs for 4 h. Each value represents means ± SD (n=3).

effectively enhance the selectivity of the nanosystem between cancer and normal cells, especially making the nanosystem specific toward multidrug cancer cells.

To evaluate the selectivity between cancer cells and drug resistant cells, internalization of couramin-6 loaded of GAL/Bor@SeNPs in HepG2 and R-HepG2 cells was examined. The cells were incubated with 30 μM GAL/Bor@SeNPs for 1 h, 2 h and 4 h, and then the cellular uptake was investigated through a fluorescence microplate reader with ex/em wavelengths set at 430 and 485 nm to measure the fluorescence intensity of couramin-6. **Fig. 4C** showed that the intracellular drug in two cell lines was time-dependent manner. The cellular uptake of GAL/Bor@SeNPs was much higher in HepG2 and R-HepG2 cells than that in LO2 human normal cells. For instance, after 4 h incubation with 30 μM GAL/Bor@SeNPs, the concentrations of GAL/Bor@SeNPs in R-HepG2 cells was found at 16.16 μM/10^8 cells, which was about two times higher than that in HepG2 cells and about 4-5 folds higher than that in LO2 cells. We also observed the relationship between higher ASGP-R expression levels in R-HepG2 cells and higher cellular uptake of R-HepG2 cells. Furthermore, to examine the role of GAL in the cellular uptake, the R-HepG2 cells were incubated with various concentrations of GAL for 2 h to saturate the ASGP receptor in the cell membrane, and then treated with GAL/Bor@SeNPs (30 μM) for 4 h. As shown in **Fig. 4D**, the uptake of the nanoparticles was significantly inhibited by addition of GAL in a dose-dependent manner. For instance, after treatment with 2 mg/L GAL for 2 h, the cellular uptake of GAL/Bor@SeNPs was 0.47 μM/10^8 cells, while that without GAL co-treatment was 17.21 μM/10^8 cells, which was lower than that of SeNPs alone. It is possible that GAL not only inhibits ASGP receptor-mediated endocytosis, but also inhibits the protein expression and functions related to other kinds of cellular uptake for nanoparticles. Taken together, these results further confirm the important role of GAL in the selective cellular uptake of the nanosystem.

To examine the role of Bor and GAL in the enhanced cellular uptake of the nanosystem, the cellular uptake of SeNPs, Bor@SeNPs and GAL@SeNPs in R-HepG2 cells was examined by using a fluorescence microplate reader. **Fig. 5A** showed that the intracellular drugs in R-HepG2 cells were time-dependent manner. For instance, after incubation with 30 μM Bor@SeNPs and GAL@SeNPs for 4 h, the intracellular Se concentration increased to 6.4 and 5.5 μM /10^8 cells respectively, which was about 2.0 and 1.7 folds higher than that of SeNPs. Furthermore, while exposed to 30 μM SeNPs alone for 4 h, the cellular uptake of SeNPs was 2.72 μM /10^8 cells (**Fig. 5B**). Interestingly, combination treatment of cells with Bor and SeNPs resulted in significant increase in cellular uptake in R-HepG2 cells (5.41 μM /10^8 cells), which was 2.0 fold higher than that of SeNPs alone. This results indicate that both Bor and GAL could enhance the cellular uptake of GAL/Bor@SeNPs.

Intracellular localization, uptake pathways and pH responsive drug release of GAL/Bor@SeNPs

Endocytosis has been identified as an important cellular uptake mechanism for nanoparticles.[17] To investigate whether GAL/Bor@SeNPs enter the cells through endocytosis mechanisms, the fluorescence microscopy analysis was taken. The intracellular localization of GAL/Bor@SeNPs in cancer cells was examined through using two specifics probes, DAPI (blue) for nucleus and Lyso Tracker Red for the lysosomes. From **Fig. 6A and B**, the overlay of red and green fluorescence demonstrated that the co-localization of lysosomes and GAL/Bor@SeNPs in R-HepG2 and HepG2cells, which demonstrated that GAL/Bor@SeNPs enter the cancer cells via lysosomes. As time increases, the green fluorescence intensity increased, indicating that the more drugs enter the cells. After 1h of incubation, the drug into the R-HepG2 cells lysosomes. For the point of 12 h, the drug released from lysosomes to the nucleus in R-HepG2 cells. Meanwhile, there was slight green fluorescence intensity in HepG2 cells for the time of 12 h. This was in good accordance with the results of cellular uptake.

To study the mechanism of cellular uptake, the cells were exposed to various endocytosis inhibitors before addition of GAL/Bor@SeNPs. As shown in **Fig. 6C**, the combination of 2-deoxy-D-glucose (DOG) and sodium azide (NaN_3) treatments, or at low temperature of 4℃, significantly decreased the cellular internalization of GAL/Bor@SeNPs to 54.29% and 70.01% of the control, which indicated that GAL/Bor@SeNPs entered R-HepG2 cells through endocytosis by energy-dependent pathways. As shown in **Fig. 6C**, dynasore, an inhibitor of dynamin-mediated

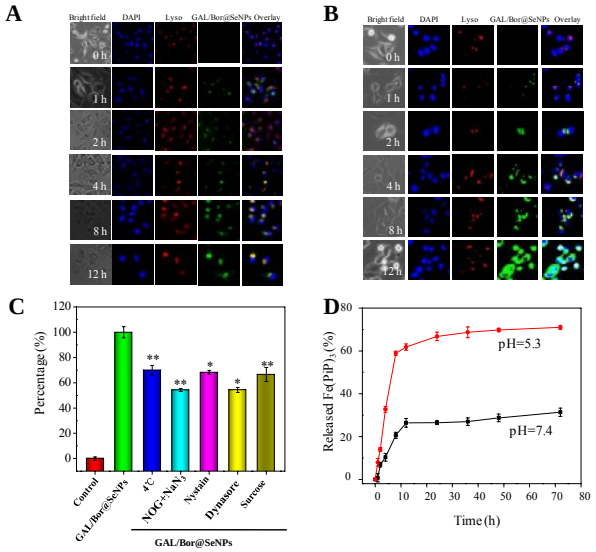

Fig. 6 (A) Intracellular trafficking of GAL/Bor@SeNPs in HepG2 cells. (B) Intracellular trafficking of GAL/Bor@SeNPs in R-HepG2 cells. The cells treated with GAL/Bor@SeNPs were stained with DAPI (nucleus) and lysotracker (lysosome) at 37 ℃ for different periods of time and visualized under a fluorescent microscope. (C) Intracellular uptake of GAL/Bor@SeNPs in R-HepG2 cells under different endocytosis-inhibited conditions. Significant difference between treatment and control groups is indicated at * P <0.05,** P < 0.01 level. (D) *In vitro* release profiles of $Fe(PiP)_3$from GAL/Bor@SeNPs in PBS solution (pH 7.4 and pH 5.3). Each value represents means ± SD (n=3).

lipid raft endocytosis, effectively inhibited the cellular uptake of the nanoparticles to 54.33% of control, indicating that dynamin-mediated is the main pathway. Meanwhile, surcose, an inhibitors of clathrin-mediated endocytosis, reduced the uptake of GAL/Bor@SeNPs to 66.60% of the control, indicated that the endocytosis of GAL/Bor@SeNPs was also included clathrin-mediated endocytosis. In addition, nystatin decreased the endocytosis of GAL/Bor@SeNPs to 68.25% of the control, demonstrating that caveolae-mediated endocytosis also involved in cellular internalization of GAL/Bor@SeNPs. Therefore, there are two pathways for GAL/Bor@SeNPs in R-HepG2 cells, including dynamin-mediated lipid raft endocytosis and clathrin-mediated endocytosis.

To understand the drug release of $Fe(PiP)_3$, the GAL/Bor@SeNPs powder was suspended in phosphate buffered solution (PBS) with pH 7.4 and pH 5.3 to imitate the environments of normal blood condition and acidic lysosomes. From **Fig. 6D**, it is found that the release of $Fe(PiP)_3$ amount was 14.02% at pH 5.3 and 10.45% at pH 7.4 within 2 h, and the release of $Fe(PiP)_3$ amount achieved to 71.01% at pH 5.3 and 31.35% at pH 7.4 for the time of 72 h. Possibly, the $Fe(PiP)_3$ complex was positively charged, while the inner layer of the nanoystem, Bor@SeNPs was negatively charged (Fig. 1F). So the $Fe(PiP)_3$ complex could be loaded into the nanoparticles through electrostatic interaction. However, under acidic environment, the proton in the solution may compete with the complex for interaction with the nanoparticle composition, leading to the release of the free complex from the nanoparticle into the solution. These results demonstrate the pH-responsive drug release property of the nanosystem.

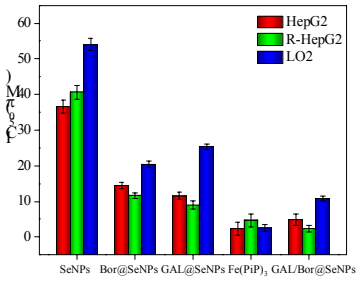

Fig. 7 Selective cytotoxicity of GAL/Bor@SeNPs in HepG2 cells, R-HepG2 cells and LO2 cells for 72 h. Each value represents means ± SD (n=3).

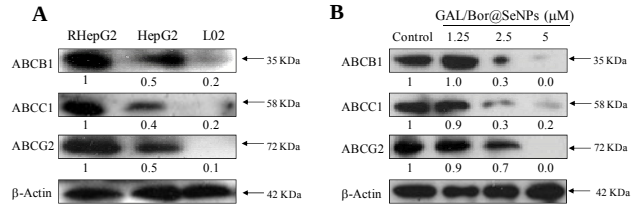

Fig. 8 (A) Difference in expression levels of ABC family proteins in R-HepG2, HepG2 and LO2 cells. (B) Effects of GAL/Bor@SeNPs on the expression levels of ABC family in R-HepG2 cells. β-actin was used as loading control.

GAL/Bor@SeNPs inhibit ABC family protein expression

To examine the role of Bor and GAL, the MTT assay was measured. As shown in **Fig. 7**, the IC_{50} of HepG2, R-HepG2 and LO2 cells were 36.6, 40.6 and 54.0 μM for SeNPs, 14.4, 11.6 and 20.3 μM for Bor@SeNPs, and 11.5, 8.9, 25.3 μM for GAL@SeNPs, respectively. The results indicate that Bor and GAL can significantly enhance the cells growth inhibitory effects of SeNPs on HepG2, R-HepG2 and LO2 cells. Compare with $Fe(PiP)_3$, GAL/Bor@SeNPs reduced the toxicity on LO2 cells and improved the activity on R-HepG2 cells. The IC_{50} of GAL/Bor@SeNPs on HepG2 was 4.88 μM, which was about 2 fold on R-HepG2. However, compared with those cancer cells, the toxicity of GAL/Bor@SeNPs in LO2 normal human liver cells (IC_{50} value: 10.8 μM) was significantly much lower. The expected results suggest that the GAL/Bor@SeNPs can be effective in treating multidrug resistant cancer cells.

Since ABC family proteins are important factors contributing to multidrug resistance in cancers. Therefore, the down-regulation of the expression levels of these proteins will be able to reverse the cancer multidrug resistance. To further determine the mechanisms accounting for the selective cellular uptake of GAL/Bor@SeNPs in R-HepG2, western blot analysis was employed to analyze the expression of ABC family proteins. The results showed that, the expression levels of these proteins in R-HepG2 cells were significantly higher than that of HepG2 cells and LO2 cells (**Fig. 8A**). We further examined the effects of GAL/Bor@SeNPs on the expression levels of ABC family protein on R-HepG2 cells. The results showed that, GAL/Bor@SeNPs effectively inhibited the expression levels of ABCB1, ABCC1 and ABCG2 in R-HepG2 cells in a dose-dependent manner (**Fig. 8B**). Consistently, previous study has showed that, Bor could participate in reversing multidrug

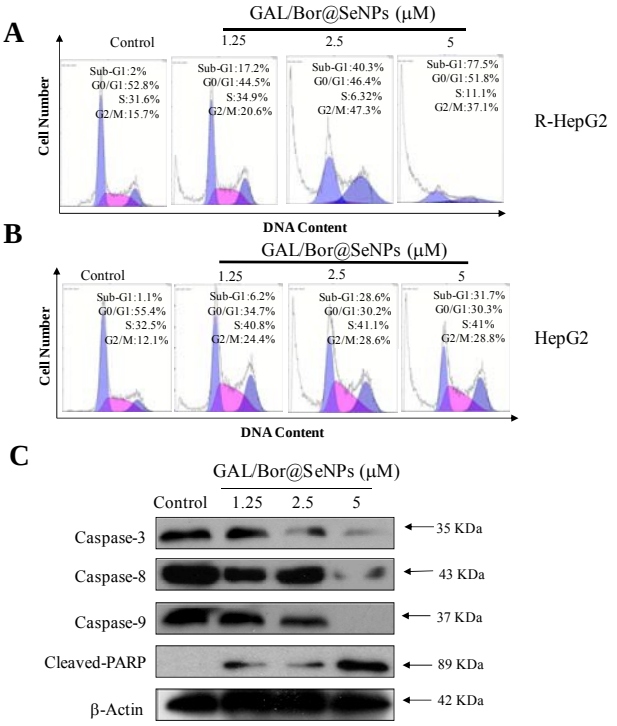

Fig. 9 (A-B) Flow cytometric analysis of GAL/Bor@SeNPs-treated in R-HepG2 and HepG2 cells for 72 h. (C) Effects of GAL/Bor@SeNPs on the expression levels of Caspase-9, Caspase-8, Caspase-3 and Cleaved-PARP. β-actin was used as loading control.

resistance by inhibition the expression of p-gp.[31] These results indicate that the GAL/Bor@SeNPs antagonize cancer multidrug resistance by inhibition of ABC family proteins.

Induction of cancer cell apoptosis by GAL/Bor@SeNPs

Apoptosis has been well demonstrated as a major action mechanism of Se.[17, 26, 43] In this study, flow cytometric analysis was performed to examine the action modes of the functionalized SeNPs. As shown in **Fig. 9A, B** and **Fig. S3**, Bor@SeNPs and GAL/Bor@SeNPs effectively induced apoptosis in R-HepG2 cells in dose-dependent manner, while GAL/Bor@SeNPs exhibited much higher apoptosis-inducing efficacy than Bor@SeNPs. For instance, the sub-G1 cell population in R-HepG2 cells exposed to 1.25-5 μM GAL/Bor@SeNPs increased from 1.2% (control) to 17.2%, 40.3% and 77.5%, which were much higher than those of HepG2 cells (6.2%, 28.6% and 31.7%). Caspases family proteases, a kind of cysteine protease, have been played a vital role in causing apoptosis of cancer cells. Therefore, Western blotting was carried out to examine the involvement of caspases family members in cell apoptosis induced by GAL/Bor@SeNPs. As shown in **Fig. 9C**, the cells treated with GAL/Bor@SeNPs demonstrated dose-dependent decrease in total caspase-3, caspase-8 and caspase-9. In contrast, the cleavage of PARP at 89 kDa, an important biochemical hallmark of apoptosis, was significantly increased in a dose-dependent manner. These results demonstrated that GAL/Bor@SeNPs induce cancer cells apoptosis by means of intrinsic and extrinsic pathways.

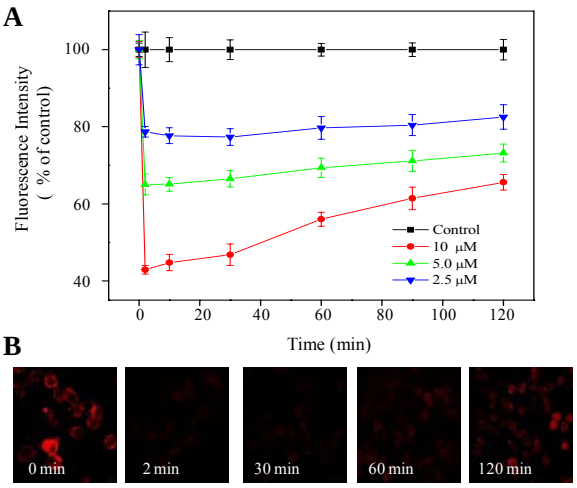

Fig. 10 Changes of ROS generation induced by GAL/Bor@SeNPs. (A) R-HepG2 cells were treated with the different concentrations of GAL/Bor@SeNPs for 120 min and the levels of the intracellular ROS were analyzed by DHE fluorescence intensity. (B) R-HepG2 cells were exposed to 10 μM DHE for 30 min, and then incubated with 10 μM GAL/Bor@SeNPs for different periods of time. Each value represents means ± SD (n=3).

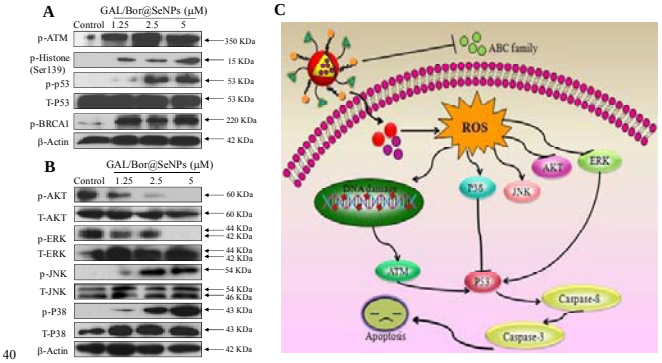

Fig. 11 Effects of GAL-SeNPs on the expression level of DNA damage and MAPKs family protein. Western blot analysis of expression levels of (A)P-ATM, P-His, P-BRCA1, T-P53, p-P53,(B) p-P38, P38, p-ERK,T-ERK, p-JNK,T- JNK, p-AKT, T-AKT treated by GAL/Bor@SeNPs. β-actin was used as loading control. (C) The apoptosis signaling pathways induced by GAL/Bor@SeNPs in R-HepG2 cells.

Activation of ROS-medicated signaling pathways by GAL/Bor@SeNPs

ROS, which encompassing hydroxyl radical, superoxide and hydrogen peroxide, plays a vital role in cells apoptosis signal way induced by chemotherapeutic agents.[50] It has been reported that the change of ROS levels can damage molecular, and furthermore can induce the cell apoptosis.[26, 44] In this study, we evaluated the intracellular ROS generation in cells exposed to GAL/Bor@SeNPs by using dihydroethidium (DHE) fluorescence decreased with a dose-dependent manner, suggesting the down-regulation of intracellular ROS generation by GAL/Bor@SeNPs. Moreover, the intracellular ROS levels were down to 42.9% at high concentration of 10 μM after 2 min of treatment, suggesting GAL/Bor@SeNPs induced cell apoptosis by inhibition of ROS generation. This conclusion was further verified by fluorescence

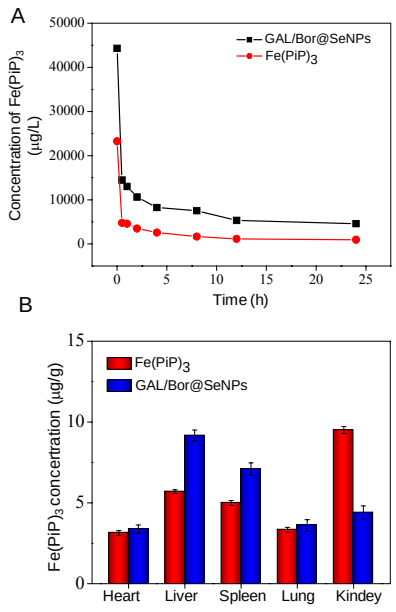

Fig. 12. (A) Concentration of $Fe(PiP)_3$ in plasma at different time after iv injection of $Fe(PiP)_3$ and GAL/Bor@SeNPs at dose of 5 mg/kg as calculated by $Fe(PiP)_3$. (B) *In vivo* biodistribution of $Fe(PiP)_3$ and GAL/Bor@SeNPs in major organs after iv injection for 72 h.

imaging. As shown in **Fig. 10B**, the decrease in fluorescent intensity of DHE probe was observed in R-HepG2 cells in a time-dependent manner after exposure to GAL/Bor@SeNPs.

Many studies have showed that ROS overproduction in cancer cells could induce apoptotic cell death by activation of different downstream signaling pathways.[3] In order to verify whether the role of GAL/Bor@SeNPs induced cell apoptosis by p53 pathway, the alterations of expression levels of proteins related to p53 probe. **Fig. 10A** showed that the DHE fluorescence intensity pathway, including p-BRCA1, p-ATM and Histone at Ser139 were determined through Western blot analysis. From **Fig. 11A**, we found that the phosphorylated p53 expression was increased significantly while total p53 expression was not changed. Moreover, when the cells pretreated with GAL/Bor@SeNPs, the protein expression of p-ATM, p-BRCA1 and Ser139-Histone H2A.X were significantly up-regulated. These results suggested that GAL/Bor@SeNPs triggers cancer cell apoptosis through ROS-activated p53 phosphorylation.

Mitogen-activated protein kinases (MAPKs), including p38, ERK and JNK, is one of the intricate signaling pathways in cells, and act as important regulators of cell proliferation, growth and apoptosis. Herein, to examine the roles of MAPKs and AKT in GAL/Bor@SeNPs-induced apoptosis, Western blot analysis was used to evaluate the effects of GAL/Bor@SeNPs on the expression levels of phosphorylated and total MAPKs and AKT apoptotic MAPKs) increased significantly in a concentration-dependent manner. On the contrary, the phosphorylation levels of antiapoptotic kinases (ERK and AKT) was effectively inhibited by treatments of GAL/Bor@SeNPs. Taken together, the expected results demonstrated that MAPK and AKT pathways were involved in cancer cell apoptosis induced by GAL/Bor@SeNPs. **Fig. 11C** have showed that the major signaling pathway of GAL/Bor@SeNPs-mediated cell apoptosis.

Pharmacokinetics and biodistribution of GAL/Bor@SeNPs

To evaluate the application potential of GAL/Bor@SeNPs *in vivo*, the pharmacokinetics and biodistribution of this nanosystem were evaluated in mice via intravenous administration. As displayed in **Fig.12A**, the two-compartment pharmacokinetics was happened in the $Fe(PiP)_3$ and GAL/Bor@SeNPs. The C_{max} of GAL/Bor@SeNPs was 1.9 times of $Fe(PiP)_3$ (**Table S1**). Moreover, the pharmacokinetics parameters of the AUC in blood with GAL/Bor@SeNPs treating was significantly increased to 5.2 folds higher than that of $Fe(PiP)_3$. Furthermore, compared with free $Fe(PiP)_3$, GAL/Bor@SeNPs remarkably prolonged the $t_{1/2\beta}$ (18.7 h) of drug, which was 2.1 folds higher than $Fe(PiP)_3$. Consequently, the clearance of GAL/Bor@SeNPs was decreased to 3.72 mL/h, which was 5.2 folds lower than that of $Fe(PiP)_3$. These results indicated that the nanosystem markedly increased the blood circulation time of $Fe(PiP)_3$ *in vivo*.

Furthermore, the mice were sacrificed after 72-h drug treatment to further investigate the biodistribution of GAL/Bor@SeNPs in different organs. As shown in **Fig. 12B**, the accumulation of $Fe(PiP)_3$ and GAL/Bor@SeNPs were less in heart and lung compared with other organs. However, the accumulation of GAL/Bor@SeNPs was increased to 9.16 μg/g and 7.09 μg/g in liver and spleen than $Fe(PiP)_3$, which could be due to the reticuloendothelial system (RES) uptake. Furthermore, the accumulation of GAL/Bor@SeNPs was 2.15 times lower than that of $Fe(PiP)_3$ in kindey, which suggest that $Fe(PiP)_3$ may be easily cleared by blood circulation. These data were consistent with the results of pharmacokinetics. Taken together, these results support the future medicinal application potential of GAL/Bor@SeNPs.

4 Conclusions

In summary, we have designed and described the fabrication and application of GAL/Bor@SeNPs in overcoming multidrug resistance. A novel actively targetable drug delivery carrier of GAL/Bor@SeNPs has been developed by conjugating GAL and Borneol onto the surface of SeNPs and loaded with $Fe(PiP)_3$ complex. GAL as a targeted ligand can significantly enhance the cellular uptake of $Fe(PiP)_3$-loaded nanoparticles through dynamin-mediated lipid raft endocytosis and clathrin-mediated endocytosis and the efficiency of anti-cancer by selectively expression of ASGP R in cancer and normal cells. Importantly, GAL/Bor@SeNPs overcame multidrug resistance in R-HepG2 cells through inhibition of ABC family proteins expression, resulting in enhanced drug accumulation and retention. Furthermore, the internalized GAL/Bor@SeNPs induced intracellular ROS variation to regulate AKT and MAPKs pathways to facilitate cell apoptosis. Moreover, this nanosystem effectively prolonged the circulation time of encapsulated drugs.Taken together, this study may provide a rational strategy for construction of functional nanosystem to reverse multidrug resistant cancers. GAL/Bor@SeNPs can be further evaluated as specific and efficient theranostic agents to against resistant cancers.

Acknowledgements

This work was supported by National High Technology Research

and Development Program of China (863 Program, SS2014AA020538), Science Foundation for Distinguished Young Scholars (S2013050014667) of Guangdong Province, Foundation for High-level Talents in Higher Education of Guangdong, Natural Science Foundation of China, Research Fund for the Doctoral Program of Higher Education of China (20114401110004), Shenzhen Basic Research Grant (JCYJ20130401152508660) and YangFan Innovative & Entepreneurial Research Team Project (201312H05).

Notes and references

Department of Chemistry, Jinan University, Guangzhou 510632, China. Fax: +86 20 85221263; Tel: +86 20-85225962;E-mail: tchentf@jnu.edu.cn

† Electronic Supplementary Information (ESI) available: [details of any supplementary information available should be included here]. See DOI: 10.1039/b000000x/

1. D. N. Heo, D. H. Yang, H.-J. Moon, J. B. Lee, M. S. Bae, S. C. Lee, W. J. Lee, I.-C. Sun and I. K. Kwon, *Biomaterials*, 2012, **33**, 856-866.
2. Y. Li, X. Li, W. Zheng, C. Fan, Y. Zhang and T. Chen, *J. Mater. Chem. B*, 2013, **1**, 6365-6372.
3. L. He, Y. Huang, H. Zhu, G. Pang, W. Zheng, Y. S. Wong and T. Chen, *Adv. Funct. Mater.*, 2014, **24**, 2754-2763.
4. F. M. Kievit, F. Y. Wang, C. Fang, H. Mok, K. Wang, J. R. Silber, R. G. Ellenbogen and M. Zhang, *J. Controlled Release*, 2011, **152**, 76-83.
5. A. Shapira, Y. D. Livney, H. J. Broxterman and Y. G. Assaraf, *Drug Resist. Updat.*, 2011, **14**, 150-163.
6. Y. Chen, H. Chen and J. Shi, *Mol. Pharm.*, 2013.
7. G. Szakács, J. K. Paterson, J. A. Ludwig, C. Booth-Genthe and M. M. Gottesman, *Nat. Rev. Drug Discov.*, 2006, **5**, 219-234.
8. Y. Guo, M. Chu, S. Tan, S. Zhao, H. Liu, B. O. Otieno, X. Yang, C. Xu and Z. Zhang, *Mol. Pharm.*, 2013, **11**, 59-70.
9. J. Shen, Q. He, Y. Gao, J. Shi and Y. Li, *Nanoscale*, 2011, **3**, 4314-4322.
10. R. Misra, S. Acharya and S. K. Sahoo, *Drug Discov. Today*, 2010, **15**, 842-850.
11. B. Subia and S. Kundu, *Nanotechnology*, 2013, **24**, 035103.
12. D. J. Schaer, P. W. Buehler, A. I. Alayash, J. D. Belcher and G. M. Vercellotti, *Blood*, 2013, **121**, 1276-1284.
13. F. Wang, D. Zhang, Q. Zhang, Y. Chen, D. Zheng, L. Hao, C. Duan, L. Jia, G. Liu and Y. Liu, *Biomaterials*, 2011, **32**, 9444-9456.
14. L. L. Li, Q. Yin, J. Cheng and Y. Lu, *Adv. Healthc. Mater.*, 2012, **1**, 567-572.
15. R. Tang, C. S. Kim, D. J. Solfiell, S. Rana, R. Mout, E. M. Velázquez-Delgado, A. Chompoosor, Y. Jeong, B. Yan and Z.-J. Zhu, *ACS nano*, 2013, **7**, 6667-6673.
16. F. Yang, Q. Tang, X. Zhong, Y. Bai, T. Chen, Y. Zhang, Y. Li and W. Zheng, *Int J Nanomedicine*, 2012, **7**, 835-844.
17. W. Liu, X. Li, Y.-S. Wong, W. Zheng, Y. Zhang, W. Cao and T. Chen, *ACS nano*, 2012, **6**, 6578-6591.
18. Y. Zhang, X. Li, Z. Huang, W. Zheng, C. Fan and T. Chen, *Nanomed. Nanotechnol. Biol. Med.*, 2013, **9**, 74-84.
19. W. Jiang, Y. Fu, F. Yang, Y. Yang, T. Liu, W. Zheng, L. Zeng and T. Chen, *Appl. Mater. Interfaces*, 2014, **6**, 13738-13748.
20. T. Gianferrara, I. Bratsos and E. Alessio, *Dalton Trans.*, 2009, 7588-7598.
21. T. Chen, Y. Liu, W.-J. Zheng, J. Liu and Y.-S. Wong, *Inorg. Chem.*, 2010, **49**, 6366-6368.
22. N. Cutillas, G. S. Yellol, C. de Haro, C. Vicente, V. Rodríguez and J. Ruiz, *Coord. Chem. Rev.*, 2013, **257**, 2784-2797.
23. S. Ramakrishnan, E. Suresh, A. Riyasdeen, M. A. Akbarsha and M. Palaniandavar, *Dalton Trans.*, 2011, **40**, 3524-3536.
24. S. Saha, D. Mallick, R. Majumdar, M. Roy, R. R. Dighe, E. D. Jemmis and A. R. Chakravarty, *Inorg. Chem.*, 2011, **50**, 2975-2987.
25. B. Lal, A. Badshah, A. A. Altaf, M. N. Tahir, S. Ullah and F. Huq, *Dalton Trans.*, 2012, **41**, 14643-14650.
26. Y. Huang, L. He, W. Liu, C. Fan, W. Zheng, Y.-S. Wong and T. Chen, *Biomaterials*, 2013, **34**, 7106-7116.
27. B. Yu, M. Ruan, X.-b. Cui, J.-M. Guo, L. Xu and X.-P. Dong, *J. Pharm. Biomed. Anal.*, 2013, **77**, 128-132.
28. X. Song, Y. Lu, R. Wen, S. Du, X. Zhao, J. Zhao and Y. Li, *Pharmazie*, 2012, **67**, 848-851.
29. J. Su, H. Lai, J. Chen, L. Li, Y.-S. Wong, T. Chen and X. Li, *PLoS ONE*, 2013, **8**, e63502.
30. Y. Zhou, W. Li, L. Chen, S. Ma, L. Ping and Z. Yang, *Environ. Toxicol. Pharmacol.*, 2010, **29**, 229-234.
31. H. He, Q. Shen and J. Li, *Arch. Pharmacal Res.*, 2011, **34**, 1161-1170.
32. B. Yu, X. Li, W. Zheng, Y. Feng, Y.-S. Wong and T. Chen, *J. Mater. Chem. B*, 2014, **2**, 5409-5418.
33. L. Pan, Q. He, J. Liu, Y. Chen, M. Ma, L. Zhang and J. Shi, *J. Am. Chem. Soc.*, 2012, **134**, 5722-5725.
34. C. Zhang, Y. Cheng, G. Qu, X. Wu, Y. Ding, Z. Cheng, L. Yu and Q. Ping, *Carbohydr. Polym.*, 2008, **72**, 390-397.
35. J. Han and Y. Il Yeom, *Int. J. Pharm.*, 2000, **202**, 151-160.
36. T. Ren, G. Zhang and D. Liu, *Tetrahedron Lett.*, 2001, **42**, 1007-1010.
37. K. Kunath, A. von Harpe, D. Fischer and T. Kissel, *J. Controlled Release*, 2003, **88**, 159-172.
38. D. Bhadra, A. Yadav, S. Bhadra and N. Jain, *Int. J. Pharm.*, 2005, **295**, 221-233.
39. Z. Shen, W. Wei, H. Tanaka, K. Kohama, G. Ma, T. Dobashi, Y. Maki, H. Wang, J. Bi and S. Dai, *Pharmacol. Res.*, 2011, **64**, 410-419.
40. Y. Wang, C.-Y. Hong and C.-Y. Pan, *Biomacromolecules*, 2013, **14**, 1444-1451.
41. D. R. Nogueira, M. Mitjans, M. Infante and M. Vinardell, *Acta Biomater.*, 2011, **7**, 2846-2856.
42. D. R. Nogueira, L. Tavano, M. Mitjans, L. Pérez, M. R. Infante and M. P. Vinardell, *Biomaterials*, 2013, **34**, 2758-2772.
43. B. Yu, Y. Zhang, W. Zheng, C. Fan and T. Chen, *Inorg. Chem.*, 2012, **51**, 8956-8963.
44. Y. Luo, X. Li, T. Chen, Y. Wang and W. Zheng, *MedChemComm*, 2012, **3**, 1143-1146.
45. X.-L. Li, T. Chen, Y.-S. Wong, G. Xu, R.-R. Fan, H.-L. Zhao and J. C. Chan, *Int. J. Biochem. Cell Biol.*, 2011, **43**, 525-534.
46. Z. Liu, A. C. Fan, K. Rakhra, S. Sherlock, A. Goodwin, X. Chen, Q. Yang, D. W. Felsher and H. Dai, *Angew. Chem. Int. Ed.*, 2009, **48**, 7668-7672.
47. L. Zhang, L. Han, J. Qin, W. Lu and J. Wang, *Pharm. Res.*, 2013, **30**, 2560-2572.
48. X. Z. Yang, X. J. Du, Y. Liu, Y. H. Zhu, Y. Z. Liu, Y. P. Li and J. Wang, *Adv. Mater.*, 2014, **26**, 931-936.
49. J. Ding, C. Xiao, Y. Li, Y. Cheng, N. Wang, C. He, X. Zhuang, X. Zhu and X. Chen, *J. Controlled Release*, 2013, **169**, 193-203.
50. Y.-C. Ou, C.-R. Yang, C.-L. Cheng, S.-L. Raung, Y.-Y. Hung and C.-J. Chen, *Eur. J. Pharmacol.*, 2007, **563**, 49-60.

Table of contents entry

This study demonstrates the construction of a cancer-targeted nanosystem as payload of iron complexes to reverse cancer multidrug resistance.